

Study of ZnS:Mn²⁺, Te²⁺ phosphor for improving the hue rendering indicator of WLEDs

Van Liem Bui¹, Nguyen Thi Phuong Loan², Phan Xuan Le³

¹Faculty of Fundamental Science, Industrial University of Ho Chi Minh City, Ho Chi Minh, Vietnam

²Faculty of Fundamental 2, Posts and Telecommunications Institute of Technology, Ho Chi Minh, Vietnam

³Faculty of Mechanical-Electrical and Computer Engineering, School of Engineering and Technology, Van Lang University, Ho Chi Minh, Vietnam

Article Info

Article history:

Received Jun 4, 2021

Revised May 28, 2022

Accepted Jun 25, 2022

Keywords:

Colour rendered indice

Dual-layer remote

Mie-scattered hypothesis

Phosphor geometry WLEDs

Zns:Mn²⁺, Te²⁺

ABSTRACT

This research combines a phosphor-in-glass (PiG) YAG:Ce³⁺ with a red liquid-type quantum dot (LQD) to invent high-quality white light-emitting diodes (WLEDs). When the PiG LQD-built WLEDs reach 100 mA, they provide heated white illumination offering an outstanding color rendering index (CRI) (Ra=93.9, R9=97.7, and R13=98.1). The luminescent efficiency (LE) and correlating chromatic temperature, correspondingly, are 62 lm/W and 3764 K. In comparison to PiG integrated with solid-kind quantum dot, it has great LE, remarkable CRI, and lower top layer temperature because of self-aggregation and impediment in the outside flaws in semiconductor quantum dots (QDs) of the solid-condition, as well as effective thermal dissipation. The findings suggest that the produced WLEDs could be potential in high-quality lighting applications.

This is an open access article under the [CC BY-SA](https://creativecommons.org/licenses/by-sa/4.0/) license.



Corresponding Author:

Phan Xuan Le

Faculty of Mechanical-Electrical and Computer Engineering, School of Engineering and Technology

Van Lang University

Ho Chi Minh City, Vietnam

Email: le.px@vlu.edu.vn

1. INTRODUCTION

Because of its configurable luminosity, large heat stability, good mechanical power, and effortlessness of production [1]–[4], phosphorus-in-glass (PiG) is a potential epoxy-free hue adapter in increased-strength white lightings including advertising white light-emitting diodes (WLEDs) and the upcoming version of laser-influenced white-emitted illumination. Yellow-emitted PiG has been developed via fusing YAG phosphorus ions in a glass substrate at low temperatures, also it has recently been used in distant-kind WLEDs [5]–[7]. Owing to a red element scarcity, YAG:PiG-based WLEDs exhibit inferior hue standards with a poor CRI 75 and a large CCT>5000 K despite their excellent illuminating effectiveness (LE>150 lm/W) [8]–[11]. To address this issue, commercialized nitride phosphors were used to provide chromaticity-adjustable PiG. Whereas this method improves the CRI of WLEDs (>80), nitride phosphors undergo chemical reactions among several glass substrates as well as heating declination throughout the mixing procedure. This causes an inferior phosphor quantum effectiveness [12], [13]. To compensate for the red spectrum, red-emitted uncommon earth or transitional-metallic particles were added to the YAG:Ce³⁺ PiG. [14], [15]. Yet, spectrum alteration of PiG-doped particles is insufficient, in which the efficiency of these PiGs would inevitably droop. On the condition that they have narrow/size-tunable radiation spectra, excellent quantum productivities, and wide absorbing spectra, semiconductor quantum dots (QDs) have recently matched attractive transmuting substances in the WLED devices [16]–[18]. The incorporation of

steady and effective red-colored CdSe/ZnS QDs with the YAG:Ce³⁺ phosphorus is a critical decision for increasing the WLED hue standard. QDs must stay within polymeric matrices to avoid oxidizing caused by the environment and to continue using the standard packaging technique for WLEDs [19], [20]. To acquire QD PiG adapters for distant-kind WLEDs, a QD-polymeric coating was created then applied to YAG:Ce³⁺ PiG structure [21]. Solid-kind QD (SQD) has a poor performance during polymer curing because of self-accumulation and interactions with the polymer matrix [22]. Additionally, the coffee ring impact makes it challenging for the goal of creating a homogeneous dispersion of QDs in polymer films.

In this study, we suggest using a PiG hue adapter in conjunction with a liquid-kind QD (LQD) to make high-grade WLEDs. The LQD is able to surmount QDs' poor performance occurred in the solid condition due to the QDs occupancy within the solution. Sher [23] constructed extremely effective as well as trustworthy models of WLEDs via combining LQDs from various hues. Because of the limitations of electrical power conversion and aggregating in the SQD, Le *et al.* [24] presented seven alternate LQDs for constructing high brightness WLEDs. Judging these works, the LQD has superior illuminating properties than the SQD with no requirements for the waste of time, sophisticated dispersal, and curing techniques. In this study, the YAG:Ce³⁺ PiG was made utilizing screening printing and reduced-heat processing. A red-emitting CdSe/ZnS QD composition was conveyed to the PiG set, which was subsequently employed in WLEDs to generate the PiG LQD. The optic performance of WLEDs based on PiG LQD was estimated and compared to WLEDs based on PiG SQD. In like manner, by examining the WLED's working temperatures under various driving currents. Over a lengthy period, the stability of WLEDs was tested.

2. METHOD

2.1. Preparation

In this study, we use a hexagonal (*wurtzite*) ZnS:Mn²⁺,Te²⁺. So, for the most precise results, the phosphor composition must be prepared as written in the Table 1. First, combine all the materials of ZnS, MnCO₃, and NH₄Br in the water. Then after the mixture dry in the air, powderize it. Before the firing process, add around 2-3 g of sulfur. The first stage requires us to burn the mixture inside capped quartz tubes with N₂ within 1 hour and approximately 900 °C. Next, admit the ZnTe, the materials will be mixed by milling or grinding. The second stage also begins by firing the mixture for 1 hour in capped quartz tubes with N₂ under 1200 °C. It will be powdered and then washed in a combination of a modest Br concentration in methanol, followed by repeated washes in pure methanol. The outcome phosphor should have the radiation hue is red, radiation maximum is 1.92 eV, radiation amplitude (FWHM) is 0.24 eV. Also, the UV stimulation effectiveness is ++(4.88 eV) and ++(3.40 eV).

Table 1. Ingredients of ZnS:Mn²⁺,Te²⁺ phosphor

Materials	By mole (%)	By grams
ZnS	94	92
MnCO ₃	3	3.5
ZnTe	3	5.8
NH ₄ Br	2	2

2.2. Scattering computation

This research used the LightTools software along with the Mie-hypothesis for purpose of building the LED layout, in which the accuracy of the findings must be double-checked [16]-[19]. After all the data on the scattering properties of phosphor particles used to support research on the influence of phosphorus ZnS:Mn²⁺,Te²⁺ on WLED at a high correlation temperature of 5600 K has been gathered, simulate WLEDs with double-layer phosphorus without delay. The production of phosphor combination ZnS:Mn²⁺,Te²⁺ and YAG:Ce³⁺ construct the in-cup phosphor structure of WLEDs is shown in Figure 1. It can be observed that the phosphor films are in the order as follows: ZnS:Mn²⁺,Te²⁺ phosphor, yellow phosphor YAG:Ce³⁺ phosphor, and silicone glues. WLEDs are made up of blue-emitting chips, a reflecting cup, phosphor films, as well as a polymer film, demonstrated by Figures 1(a) to (d). The reflector's parameters covering the chips have a 2.07 mm deepness, an 8 mm base, and a 9.85 mm length at the peak covering. At a maximum wavelength of 453 nm, every 9 blue chips have a radiation strength of 1.16 W. ZnS:Mn²⁺,Te²⁺ phosphor has a refractive index of 1.85, while YAG:Ce³⁺ is 1.83. In order to poise the volatility of ZnS:Mn²⁺,Te²⁺ concentration and maintain mean CCTs, the YAG:Ce³⁺ concentration must be adjusted suitably.

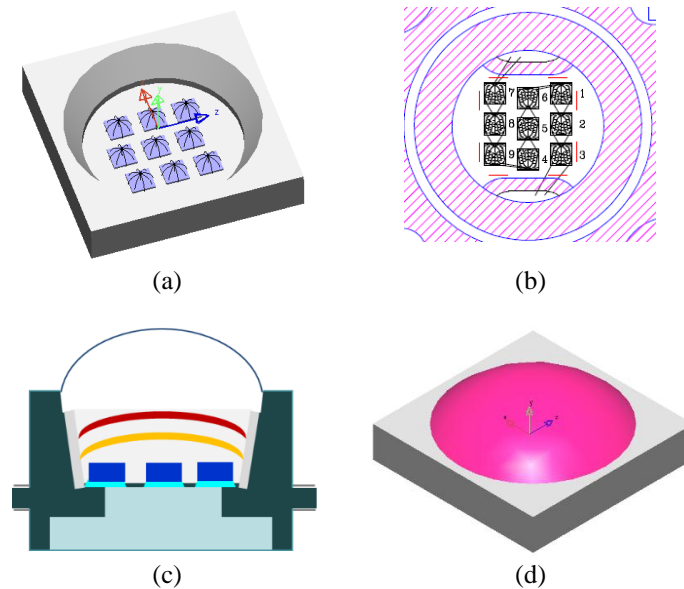


Figure 1. WLED dual-layer phosphor patterns: (a) three-dimensional layout; (b) bond formation graph; (c) cross-section prototype of pc-WLEDs; and (d) depiction of WLEDs generated using Light Tools commercial program

3. RESULTS AND DISCUSSION

As $\text{ZnS:Mn}^{2+}, \text{Te}^{2+}$ grows, the phosphorous of YAG:Ce^{3+} changes to preserve the median CCTs, see Figure 2. As an illustration, if the $\text{ZnS:Mn}^{2+}, \text{Te}^{2+}$ concentration rises from 2%-26% wt., the YAG:Ce^{3+} phosphorus have to decrease to maintain the mean CCT, which is precise for WLEDs at 5600 K. The shift relies on these findings impacts diffusing and absorptivity qualities as well, potentially improving the hue standard and light performance of WLEDs. Accordingly, the concentration of $\text{ZnS:Mn}^{2+}, \text{Te}^{2+}$ phosphor is critical, as this phosphor determines the performance of WLEDs.

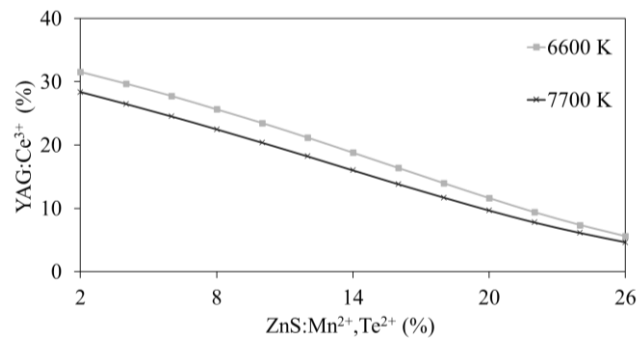


Figure 2. Stabilizing CCT's mean value using the poise among two different phosphorus concentrations

Figure 3 shows the influences of red phosphor $\text{ZnS:Mn}^{2+}, \text{Te}^{2+}$ concentrations of 2 percent and 24 percent upon WLEDs radiation spectrum. When a WLED's illuminating beam hits 5600 K ACCT, the spectral areas emit white light. The red line grows with $\text{ZnS:Mn}^{2+}, \text{Te}^{2+}$ concentration in three distinct portions, the most notable of which is from 648 to 738 nm, followed by 420-480 and 500-640 nm. When the dispersed blue emission declines within the 420-480 nm radiation range, the standard improves. The hue temperature influences the radiation spectrum's enlargement. The results reveal that the inclusion of $\text{ZnS:Mn}^{2+}, \text{Te}^{2+}$ at low (6600 K) and great (7700 K) hue temperatures considerably improves the hue standard of WLEDs. This significant discovery will influence the way producers select the optimal concentration while producing LEDs. The illuminating beam of these WLEDs is a slight drawback in those featuring excellent hue fidelity which producers should be aware of.

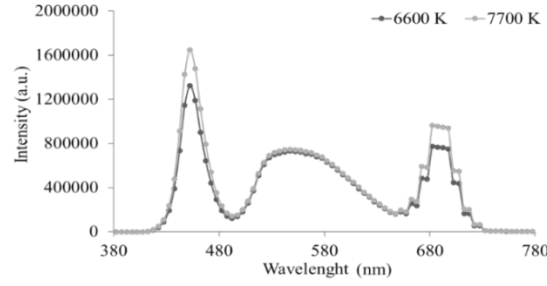


Figure 3. WLEDs emitting spectra corresponding to $\text{ZnS:Mn}^{2+}, \text{Te}^{2+}$ concentration

Because of the red phosphor $\text{ZnS:Mn}^{2+}, \text{Te}^{2+}$ absorption feature, the findings in Figure 4 imply that applying $\text{ZnS:Mn}^{2+}, \text{Te}^{2+}$ phosphor may raise the hue rendering indicator. Although the red phosphor $\text{ZnS:Mn}^{2+}, \text{Te}^{2+}$ imbibes the light of yellow as well, the absorption of the light of blue is more prevalent owing to the material phosphor properties. Whenever the package includes the red phosphor $\text{ZnS:Mn}^{2+}, \text{Te}^{2+}$, the red lighting element in WLEDs increases, which benefits CRI. One of the really popular factors used to assess the standard of a WLED is CRI; the greater the CRI, the higher the WLED's standard, and hence the more expensive the manufacturing expenses are. With the low cost of using $\text{ZnS:Mn}^{2+}, \text{Te}^{2+}$ phosphor, WLEDs with $\text{ZnS:Mn}^{2+}, \text{Te}^{2+}$ phosphor will be utilized more frequently. Because CRI is not a very in-depth indicator, it is no longer significant for assessing the hue standard of WLEDs. Instead, the CQS becomes a more precise and effective indicator of WLED efficacy. CQS is presently the most comprehensive color quality index because it measures three aspects of WLEDs: hue rendering indicator, observer choice, and hue coordination. The influence of the red phosphor $\text{ZnS:Mn}^{2+}, \text{Te}^{2+}$ on the CQS is shown in Figure 5, illustrating that it increases hue standard. Although the $\text{Ca}_5\text{B}_2\text{SiO}_{10}:\text{Eu}^{3+}$ phosphor increases hue standard, it also reduces the intensity of illumination emitted noticeably. In the following section, the numerical formulation of transferred blue-emitted light with transformed yellow-emitted light in the dual-film phosphorus configuration, a possible portion that can improve LED effectiveness, is shown as: The asymmetrical SPD of a monochromatic LED is commonly represented by a Gaussian function [22], [23]:

$$P_\lambda = P_{opt} \frac{1}{\sigma\sqrt{2\pi}} \exp \left[-0.5 * \frac{(\lambda - \lambda_{peak})^2}{\sigma^2} \right] \quad (1)$$

In which σ is determined by maximum wavelengths λ_{peak} an FWHM $\Delta\lambda$ is defined below:

$$\sigma = \frac{\lambda^2_{peak} \Delta E}{2hc\sqrt{2} \ln 2} = \frac{\lambda^2_{peak} \left(\frac{hc}{\lambda_1} - \frac{hc}{\lambda_2} \right)}{2hc\sqrt{2} \ln 2} = \frac{\lambda^2_{peak} (hc\Delta\lambda)}{2hc\sqrt{2} \ln 2} \quad (2)$$

The blue-and-yellow spectrum's aggregation can theoretically be expressed as WLED's SPD using YAG yellow phosphorous and a blue LED chip. Practically, however, the purported yellow phosphorus generates illumination in both yellow and green wavelengths (illustrated in the purposive spectrum in Figures 1 and 2). The feature that distinguishes the considerably calculated SPD from twofold shading (blue, yellow) ranging modeling might be stated to be a greenish ranging if we select a blue-emitting and yellow-emitting ranging. Finally, a green-emitting ranging might couple with the two-ranging simulation, yielding the exploratory trispectrum (B-G-Y) model (3), which remodels as (4).

$$P_\lambda = P_{opt_b} \frac{1}{\sigma_b\sqrt{2\pi}} \exp \left[-0.5 * \frac{(\lambda - \lambda_{peak_b})^2}{\sigma_b^2} \right] + P_{opt_g} \frac{1}{\sigma_g\sqrt{2\pi}} \exp \left[-0.5 * \frac{(\lambda - \lambda_{peak_g})^2}{\sigma_g^2} \right] \\ + P_{opt_y} \frac{1}{\sigma_y\sqrt{2\pi}} \exp \left[-0.5 * \frac{(\lambda - \lambda_{peak_y})^2}{\sigma_y^2} \right] \quad (3)$$

$$P_\lambda = \eta_b P_{opt_total} \frac{1}{\sigma_b\sqrt{2\pi}} \exp \left[-0.5 * \frac{(\lambda - \lambda_{peak_b})^2}{\sigma_b^2} \right] \\ + \eta_g P_{opt_total} \frac{1}{\sigma_g\sqrt{2\pi}} \exp \left[-0.5 * \frac{(\lambda - \lambda_{peak_g})^2}{\sigma_g^2} \right] \\ + \eta_y P_{opt_total} \frac{1}{\sigma_y\sqrt{2\pi}} \exp \left[-0.5 * \frac{(\lambda - \lambda_{peak_y})^2}{\sigma_y^2} \right] \quad (4)$$

where P_λ is spectrum power dispersion (SPD) (mW/nm), h is Planck's absolute (J.s), c is illumination pace (ms^{-1}), λ is wavelength (nm), P_{opt} is optic intensity (W), λ_{peak} is peak of wavelength (nm), $\Delta\lambda$ is fullfilled-width at half of maximum value (FWHM) (nm), η is dimensionless proportion of specialized spectrum to white-emitted spectrum, P_{opt_b} , P_{opt_g} , P_{opt_y} , and $P_{\text{opt}_{\text{total}}}$ is optic intensity (W) of the blue-emitted, green-emitted, yellow-emitted, and white-emitted spectrum, accordingly, λ_{peak_b} , λ_{peak_g} , and λ_{peak_y} is peak of wavelengths (nm) of the blue-emitted, green-emitted, and yellow-emitted spectrum, accordingly, σ_b , σ_g , and σ_y is FWHM-based coefficients (nm) of the blue-emitted, green-emitted, and yellow-emitted spectrum, accordingly, η_b , η_g , and η_y is dimensionless proportion of blue-green-yellow (B-G-Y) spectrum to white emitted spectrum, λ_1 , λ_2 is half-peak-intensity wavelengths.

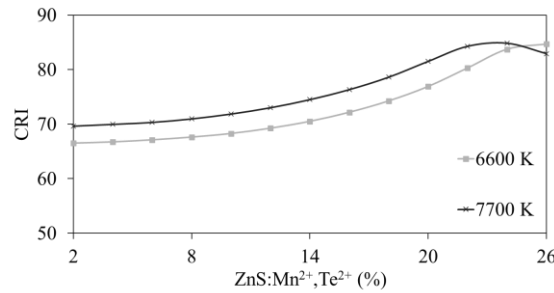


Figure 4. WLEDs colour rendered indicator relating $\text{ZnS:Mn}^{2+},\text{Te}^{2+}$ concentration

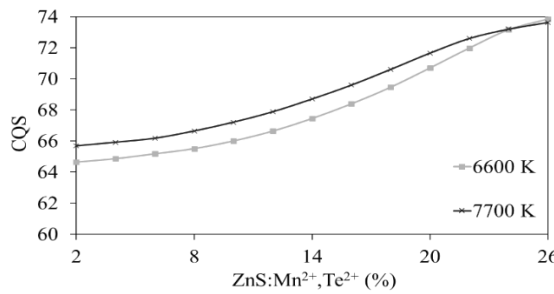


Figure 5. WLEDs hue standard ratio relating $\text{ZnS:Mn}^{2+},\text{Te}^{2+}$ concentration

Ordinarily, a spectrum that has three colors can state as SPD modeling for phosphor-coated WLEDs, which potentially is an extended Gaussian model. The Mie-theory helped us determine the diffusing of $\text{ZnS:Mn}^{2+},\text{Te}^{2+}$ phosphor particles. Correspondingly, utilizing the Mie hypothesis, the diffusing cross-section C_{sca} of spherical fragments could be determined using the calculation as follows [24]. We can also apply the Lambert-Beer law to compute the transmitted illuminating power [25]:

$$I = I_0 \exp(-\mu_{\text{ext}}L) \quad (5)$$

The direct illuminating energy is I_0 , L is the phosphorus layer thickness (mm), and the extinction factor is μ_{ext} , which could be calculated using the following formula: $\mu_{\text{ext}} = N_r C_{\text{ext}}$, where N_r denotes the particle dispersion (mm^{-3}), and C_{ext} (mm^2) is the phosphor particle extinction cross-section. The result of implementing (5) reveals that a dual-film distant phosphor configuration produces significantly more lighting beams than a single-film phosphor configuration. Henceforth, the dual-film phosphor configuration works hard and contributes to increased illuminating beam in WLEDs. The concentration of $\text{ZnS:Mn}^{2+},\text{Te}^{2+}$ has a significant impact on the optic output of double-layer phosphorus configuration WLEDs featuring red-emitting phosphorus $\text{ZnS:Mn}^{2+},\text{Te}^{2+}$. The Lambert-Beer law shows that the extinction factor μ_{ext} and the concentration of $\text{ZnS:Mn}^{2+},\text{Te}^{2+}$ rise in lockstep; nevertheless, the illumination radiation power rises in the opposite course of the extinction factor μ_{ext} . Consequently, the increase of phosphor sheet breadth by adding additional $\text{Ca}_5\text{B}_2\text{SiO}_{10}:\text{Eu}^{3+}$ reduces the luminous flux of WLEDs. Figure 6 illustrates this conclusion by reducing illuminating beam in all CCTs as the $\text{ZnS:Mn}^{2+},\text{Te}^{2+}$ concentration rises to 26%. In general, adopting a dual-film phosphor configuration with red phosphor $\text{ZnS:Mn}^{2+},\text{Te}^{2+}$ produced a significantly more illuminating beam than a single-film. Equally, $\text{ZnS:Mn}^{2+},\text{Te}^{2+}$ also provides numerous CRI and CQS improvements. Under those

circumstances, the benefits of a minor reduction in luminous flux outweigh the disadvantages. The manufacturer will determine the most appropriate concentration setting, and the optimal concentration of ZnS:Mn²⁺,Te²⁺ can neither suit the quality desires of them in the mass manufacturing of WLEDs.

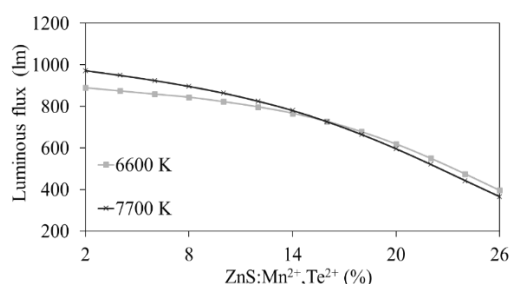


Figure 6. The lumen output of WLEDs corresponding to ZnS:Mn²⁺,Te²⁺ concentration

4. CONCLUSION

We created high-grade WLEDs via coupling a YAG:Ce³⁺ PiG and a red-emitting LQD in this study. The LQD relocated in a PiG packaging gap to prevent oxygen and humidity from interacting with the QDs. At 100 mA current, the PiG LQD-based WLED emits a warming white-emitting illumination comprising an exceptional hue standard, a 3764 K CCT, and a 62 lm/W LE. Because of the suppression of self-accumulation and outer side of QDs solid state's flaws, the PiG LQD shows a more elevated LE with better CRI than the PiG SQD. Given its superior thermal management, the PiG LQD has a reduced exterior temperature, this adds to the heating steadiness of PiG LQD-built WLEDs.

ACKNOWLEDGEMENTS

This study was financially supported by Van Lang University, Vietnam.




REFERENCES

- [1] N. V. Bharathi, T. Jeyakumaran, S. Ramaswamy and S. S. Jayabalakrishnan, "Synthesis and characterization of self-activated Ba₂V₂O₇ nanophosphor: a potential material for W-LED applications," *Mater. Res. Express*, vol. 6, pp. 106202, 2019, doi: 10.1088/2053-1591/ab3c1d.
- [2] H. Ming, J. Zhang, L. Liu, J. Peng, F. Du and X. Ye, "Luminescent Properties of a Cs₃AlF₆:Mn⁴⁺ Red Phosphor for Warm White Light-Emitting Diodes," *ECS J. Solid State Sci. Technol.*, vol. 7, pp. R149, 2018, doi: 10.1149/2.0271809jss.
- [3] T. Jansen, J. Gorobez and T. Jüstel, "Communication—Optical Properties of Red Emitting HK₃SnF₈:Mn⁴⁺ as a Color Converter for Next Generation Warm White LEDs," *ECS J. Solid State Sci. Technol.*, vol. 7, pp. R111, 2018, doi: 10.1149/2.0311806jss.
- [4] Q. Wang *et al.*, "Monolithic semi-polar InGaN/GaN near white light-emitting diodes on micro-stripped Si (100) substrate," *Chinese Phys. B*, vol. 28, pp. 087802, 2019, doi: 10.1088/1674-1056/28/8/087802.
- [5] K. K. Gupta, S. Som and C. H. Lu, "Synthesis and luminescence characterization of Ce³⁺ activated Y₂CaAl₂MgZr₂O₁₂ garnet phosphor for white light emitting diodes," *Mater. Res. Express*, vol. 6, pp. 125540, 2019, doi: 10.1088/2053-1591/ab62eb.
- [6] Y. Zhuang *et al.*, "Effect of phosphor sedimentation on photochromic properties of a warm white light-emitting diode," *J. Semicond.*, vol. 39, pp. 124006, 2018, doi: 10.1088/1674-4926/39/12/124006/pdf.
- [7] C. Sun *et al.*, "Highly efficient Mn-doped CsPb(Cl/Br)₃ quantum dots for white light-emitting diodes," *Nanotechnology*, vol. 31, pp. 065603, 2020, doi: 10.1088/1361-6528/ab5074.
- [8] X. Yang, M. Zhang, H. Ma, X. Xu and X. Yu, "Self-Crystallized Ba₂LaF₇ Glass Ceramics with High Thermal-Stability for White Light-Emitting-Diodes and Field Emission Displays," *ECS J. Solid State Sci. Technol.*, vol. 8, pp. R127, 2019, doi: 10.1149/2.0151910jss.
- [9] A. Floriduz, and J. D. Devine, "Modelling of proton irradiated GaN-based high-power white light-emitting diodes," *Jpn. J. Appl. Phys.*, vol. 57, pp. 080304, 2018, doi: 10.7567/JJAP.57.080304.
- [10] D. T. Khan *et al.*, "Study on luminescent properties of Tb³⁺ and Sm³⁺ co-doped CaSiO₃ phosphors for white light emitting diodes," *Mater. Res. Express*, vol. 7, pp. 016507, 2020, doi: 10.1088/2053-1591/ab5ab8.
- [11] C. Chen *et al.*, "Flexible inorganic CsPbI₃ perovskite nanocrystal-PMMA composite films with enhanced stability in air and water for white light-emitting diodes," *Nanotechnology*, vol. 31, pp. 225602, 2020, doi: 10.1088/1361-6528/ab7648.
- [12] Y. Zhang, J. Xu, B. Yang, Q. Cui and T. Tian, "Luminescence properties and energy migration mechanism of Eu³⁺ activated Bi₄Si₃O₁₂ as a potential phosphor for white LEDs," *Mater. Res. Express*, vol. 5, pp. 026202, 2018, doi: 10.1088/2053-1591/aaab8a.
- [13] B. G. Kumar *et al.*, "Structural control of InP/ZnS core/shell quantum dots enables high-quality white LEDs," *Nanotechnology*, vol. 29, pp. 345605, 2018, doi: 10.1088/1361-6528/aac8c9.
- [14] F. Xu *et al.*, "High performance GaN-based hybrid white micro-LEDs integrated with quantum-dots," *J. Semicond.*, vol. 41, pp. 032301, 2020, doi: 10.1088/1674-4926/41/3/032301.
- [15] A. K. Dubey, V. Kumar, M. Gupta, and D. S. Mehta, "Thermally stable laser-driven phosphor converted white light source using multilayer structured diffuser system," *Laser Phys. Lett.*, vol. 17, pp. 126001, 2020, doi: 10.1088/1612-202x/abc759.
- [16] N. T. P. Loan, D. L. Pham and N. D. Q. Anh, "Enhancement of color quality scale and luminous flux of white LEDs with remote




- phosphor geometries," *IOP Conf. Ser.: Mater. Sci. Eng.*, vol. 617, pp. 012014, 2019, doi: 10.1088/1757-899X/617/1/012014.
- [17] A. Ali *et al.*, "Blue Laser Diode-Based Remote Solid-State Lighting Using Plastic Optical Fiber and Phosphor Film for a Hazardous Environment," *ECS J. Solid State Sci. Technol.*, vol. 10, pp. 016001, 2021, doi: 10.1149/2162-8777/abd51b.
- [18] A. Lenef, M. Raukas, J. Wang and C. Li, "Phosphor Performance under High Intensity Excitation by InGaN Laser Diodes," *ECS J. Solid State Sci. Technol.*, vol. 9, pp. 016019, 2020, doi: 10.1149/2.0352001JSS.
- [19] L. Rosso, S. Tabandeh, G. Beltramino and V. Fericola, "Validation of phosphor thermometry for industrial surface temperature measurements," *Meas. Sci. Technol.*, vol. 31, pp. 034002, 2020, doi: 10.1088/1361-6501/ab4b6b.
- [20] A. K. Dubey, M. Gupta, V. Kumar, V. Singh and D. S. Mehta, "Blue laser diode-pumped Ce:YAG phosphor-coated cylindrical rod-based extended white light source with uniform illumination," *Laser Phys.*, vol. 29, pp. 056203, 2019, doi: 10.1088/1555-6611/ab05c0.
- [21] F. Garcia-Santamaria, J. E. Murphy, A. A. Setlur and S. P. Sista, "Concentration Quenching in $K_2SiF_6:Mn^{4+}$ Phosphors," *ECS J. Solid State Sci. Technol.*, vol. 7, pp. R3030, 2018, doi: 10.1149/2.0081801jss.
- [22] Y. H. Kim, N. S. M. Viswanath, S. Unithrattil, H. J. Kim and W. B. Im, "Review—Phosphor Plates for High-Power LED Applications: Challenges and Opportunities toward Perfect Lighting," *ECS J. Solid State Sci. Technol.*, vol. 7, pp. R3134, 2018, doi: 10.1149/2.0181801jss.
- [23] P. S. Dutta, "Full Spectrum Phosphors for White LEDs and Virtual Windows for Light and Health Applications," *ECS J. Solid State Sci. Technol.*, vol. 9, pp. 016023, 2020, doi: 10.1149/2.0422001JSS.
- [24] A. Mendieta, B. Fond, P. Dragomirov and F. Beyrau, "A delayed gating approach for interference-free ratio-based phosphor thermometry," *Meas. Sci. Technol.*, vol. 30, pp. 074002, 2019, doi: 10.1088/1361-6501/ab1b0c.
- [25] S. K. Maurya, R. Kushawaha, S. P. Tiwari, A. Kumar, K. Kumar and J. C. G. E. da Silva, "Thermal decomposition mediated Er^{3+}/Yb^{3+} codoped $NaGdF_4$ upconversion phosphor for optical thermometry," *Mater. Res. Express*, vol. 6, pp. 086211, 2019, doi: 10.1088/2053-1591/ab20b4.

BIOGRAPHIES OF AUTHORS






Van Liem Bui    received a Bachelor of Mathematical Analysis and master's in mathematical Optimization, Ho Chi Minh City University of Natural Sciences, VietNam. Currently, He is a lecturer at the Faculty of Fundamental Science, Industrial University of Ho Chi Minh City, Viet Nam. His research interests are mathematical physics. He can be contacted at email: buivanliem@iuh.edu.vn.



Nguyen Thi Phuong Loan    was born in Da Nang province. In 2006, She received her master degree from University of Natural Sciences. Her research interest is optoelectronics. She has worked at the Faculty of Fundamental 2, Posts and Telecommunications Institute of Technology, Ho Chi Minh City, Vietnam. She can be contacted at email: ntploan@ptithcm.edu.vn and nguyenthiphuongloan8899@gmail.com.



Phan Xuan Le    received a Ph.D. in Mechanical and Electrical Engineering from Kunming University of Science and Technology, Kunming city, Yunnan province, China. Currently, He is a lecturer at the Faculty of Engineering, Van Lang University, Ho Chi Minh City, Viet Nam. His research interests are optoelectronics (LED), power transmission and automation equipment. He can be contacted at email: le.px@vlu.edu.vn and phanxuanle.ts@gmail.com.